Structural basis for the regulation of nuclear import of Epstein-Barr virus nuclear antigen 1 (EBNA1) by phosphorylation of the nuclear localization signal

Ryohei Nakada [a], Hidemi Hirano [a,b], and Yoshiyuki Matsuura [a,b,*]

[a]Division of Biological Science, and [b]Structural Biology Research Center, Graduate School of Science, Nagoya University, Japan.

* Corresponding author at: Division of Biological Science, Graduate School of Science, Nagoya University, Furo-cho, Chikusa-ku, Nagoya 464-8602, Japan.

Tel: +81 52 789 2585 Fax: +81 52 789 2989

E-mail: matsuura.yoshiyuki@d.mbox.nagoya-u.ac.jp

Abstract

Epstein-Barr virus (EBV) nuclear antigen 1 (EBNA1) is expressed in every EBV-positive tumor and is essential for the maintenance, replication, and transcription of the EBV genome in the nucleus of host cells. EBNA1 is a serine phosphoprotein, and it has been shown that phosphorylation of S385 in the nuclear localization signal (NLS) of EBNA1 increases the binding affinity to the nuclear import adaptor importin-α1 as well as importin-α5, and stimulates nuclear import of EBNA1. To gain insights into how phosphorylation of the EBNA1 NLS regulates nuclear import, we have determined the crystal structures of two peptide complexes of importin-α1: one with S385-phosphorylated EBNA1 NLS peptide, determined at 2.0 Å resolution, and one with non-phosphorylated EBNA1 NLS peptide, determined at 2.2 Å resolution. The structures show that EBNA1 NLS binds to the major and minor NLS-binding sites of importin-α1, and indicate that the binding affinity of the EBNA1 NLS to the minor NLS-binding site could be enhanced by phosphorylation of S385 through electrostatic interaction between the phosphate group of phospho-S385 and K392 of importin-α1 (corresponding to R395 of importin-α5) on armadillo repeat 8.

Keywords: nuclear import; importin; NLS; EBNA1; Epstein-Barr virus

1. Introduction

Epstein-Barr virus (EBV) is a ubiquitous human herpes virus associated with a diverse range of tumors of both lymphoid and epithelial origin [1]. EBV nuclear antigen 1 (EBNA1) is a DNA-binding protein expressed in every EBV-positive tumor. EBNA1 plays an essential role in the maintenance and replication of the episomal EBV genome through its direct interaction with sequences in the EBV latent origin of replication (oriP) [2-5], and also acts as a transcriptional regulator [6,7]. It has been shown that EBNA1 induces B cell lymphomas in transgenic mice [8], enhances cell survival [9], and induces genetic instability [10], indicating that EBNA1 might contribute directly to oncogenesis. EBNA1 is phosphorylated at multiple serine residues when expressed in human and insect cells [11-14]. Although the physiological significance of EBNA1 phosphorylation remains incompletely understood, it has been suggested that phosphorylation of EBNA1 serine residues contributes to segregation and maintenance of the EBV genome, transcriptional activation, and nuclear import of EBNA1 [15-18].

Transport of macromolecules between the cytoplasm and nucleus occurs through nuclear pore complexes (NPCs) [19]. Eukaryotic cells control and finely tune many biological processes by regulating nuclear transport [20]. Phosphorylation of cargoes has emerged as one of the important mechanisms to regulate a multitude of nuclear transport pathways [20], including the importin (Imp) α:β-dependent nuclear import pathway [21,22]. The Impα adaptor proteins bind cargo proteins possessing the nuclear localization signal (NLS), and heterodimerize with Impβ through the N-terminal Impβ-binding (IBB) domain, forming the heterotrimeric Impα:β:NLS-cargo complexes that permeate through NPCs and deliver NLS-cargoes into the nucleus [19-22]. Mammalian cells have at least seven Impα isoforms, whose expression is tightly

regulated depending on cell type and developmental stage [23,24]. Each isoform of Impα has different substrate specificity, and many cellular and viral cargoes have been shown to associate preferentially with specific isoforms of Impα [23,24].

Previous cell biological and biochemical studies identified the NLS of EBNA1 (^{379}KRPRSPSS^{386}) [25] and demonstrated that EBNA1 binds to the nuclear import adaptor Impα1 [26-28] as well as Impα5 [28]. The amino-terminal K379 and R380 of the EBNA1 NLS are essential for nuclear translocation [18]. Although the serine residues (S383, S385, and S386) are not essential for the EBNA1 NLS, both S383 and S385 are important for nuclear translocation [18]. Phosphorylation of S385 increases nuclear import efficiency [18] and also increases the binding affinity of the EBNA1 NLS to Impα1 as well as Impα5 [18,29]. In this study, we used X-ray crystallography to elucidate how phosphorylation of EBNA1 NLS can regulate its interaction with Impα.

2. Materials and methods

2.1 Preparation of protein-peptide complexes for crystallization

N-terminally His_6- and S-tagged ΔIBB Impα1 (mouse, residues 70-529) was expressed from pET30a (Novagen) [30] in the *E. coli* host strain BL21-CodonPlus(DE3)RIL (Stratagene), and was purified over Ni-NTA (Novagen) and gel filtration over Superdex200 (GE Healthcare). S385-phosphorylated EBNA1 NLS peptide ^{378}EKRPRPRSP-pS-S^{386} (pS stands for phosphoserine) and non-phosphorylated EBNA1 NLS peptide ^{378}EKRPRPRSPSS^{386} were synthesized by GenScript. Prior to crystallization, ΔIBB Impα1 and the NLS peptide were mixed in a molar ratio of 1:3 in 10 mM Tris-HCl (pH 7.5), 150 mM NaCl, and 2 mM 2-mercaptoethanol.

2.2 X-ray crystallography

Crystals of ΔIBB Impα1 bound to S385-phosphorylated EBNA1 NLS peptide were grown at 20 °C from 0.2 mM ΔIBB Impα1 and 0.6 mM NLS peptide by hanging drop vapor diffusion against 0.1 M MES (pH 6.5), 0.9 M sodium citrate, and 10 mM DTT. Crystals of ΔIBB Impα1 bound to non-phosphorylated EBNA1 NLS peptide were grown at 20 °C from 0.2 mM ΔIBB Impα1 and 0.6 mM NLS peptide by hanging drop vapor diffusion against 0.1 M MES (pH 6.5), 0.8 M sodium citrate, and 10 mM DTT. Crystals were cryoprotected using mother liquor containing 23% glycerol, and flash-cooled in liquid nitrogen. X-ray diffraction datasets were collected at 95 K at Photon Factory beamline BL-17A using a Pilatus3 S6M detector. Diffraction data were processed using MOSFLM and CCP4 programs [31]. The structures were solved by molecular replacement using MOLREP [32] using the structure of ΔIBB Impα1 bound to Bimax1 NLS peptide (PDB code, 3UKW) [33] as a search model. The structures

were refined by iterative cycles of model building using COOT [34] and refinement using REFMAC5 [35] and PHENIX [36]. MolProbity [37] was used to validate the final models. Structural figures were produced using CCP4MG [38] and PyMOL [39]. Coordinates and structure factors have been deposited in the Protein Data Bank (PDB) with accession codes 5WUM (ΔIBB Impα1 bound to S385-phosphorylated EBNA1 NLS peptide) and 5WUN (ΔIBB Impα1 bound to non-phosphorylated EBNA1 NLS peptide).

3. Results and discussion

3.1 Crystal structure of Impα1 bound to S385-phosphorylated EBNA1 NLS peptide

We obtained crystals of the NLS-binding armadillo (ARM) repeat domain of Impα1 bound to the S385-phosphorylated NLS peptide of EBNA1, and determined the structure at 2.0 Å resolution by molecular replacement (Table 1). The structure was refined to free and working *R*-factor values of 21.2% and 18.6%, respectively. Residues 378-385 and 378-383 of the NLS peptide bound to the minor and major NLS-binding sites, respectively, were identified unambiguously in the electron density map (Fig. 1A and B). Notably, the electron density of the phosphorylated side chain of pS385 was clearly visible at the minor site (Fig. 1A), but this phosphoserine was not visible at the major site (Fig. 1B). The NLS peptides bound along the inner concave surface of Impα1 in almost fully extended conformations (Fig. 2A) and formed an extensive network of interactions with the surface residues of Impα1 (Fig. 3A-3D).

At the minor NLS-binding site (Fig. 3A, 3C, and 3D), the positively charged side chains of EBNA1 fitted into three acidic pockets on Impα1: $K379^{EBNA1}$ made hydrogen bonds with the side chain of $T328^{Imp_{\alpha}1}$ and the main-chain carbonyls of $V321^{Imp_{\alpha}1}$ and $N361^{Imp_{\alpha}1}$; $R380^{EBNA1}$ was sandwiched between the indole rings of $W399^{Imp_{\alpha}1}$ and $W357^{Imp_{\alpha}1}$ and formed a salt bridge with $E396^{Imp_{\alpha}1}$; $R382^{EBNA1}$ made a hydrogen bond with $N319^{Imp_{\alpha}1}$ and a bidentate salt bridge with $E354^{Imp_{\alpha}1}$. Although $pS385^{EBNA1}$ was not in direct contact with Impα1 residues, the negatively charged phosphate group of the $pS385^{EBNA1}$ side chain was involved in long-range electrostatic interactions with positively charged side chain of $K392^{Imp_{\alpha}1}$, which was positioned 4.5 Å from one of the phosphate oxygen atoms of $pS385^{EBNA1}$. It appears that the position and

orientation of the pS385^{EBNA1} side chain was stabilized by the electrostatic interaction with K392$^{Imp_{\alpha}1}$ and also by an intramolecular hydrogen bond between the side chain of S383^{EBNA1} and the γ oxygen atom of pS385^{EBNA1}. Thus, the positive and negative charges of the S385-phosphorylated EBNA1 NLS were complemented electrostatically by oppositely charged residues of Impα1. In addition, hydrogen bonds were made between the main chain of R380^{EBNA1} and the side chains of N361$^{Imp_{\alpha}1}$ and W357$^{Imp_{\alpha}1}$.

At the major NLS-binding site (Fig. 3B), K379^{EBNA1} formed a salt bridge with D192$^{Imp_{\alpha}1}$ and a hydrogen bond with T155$^{Imp_{\alpha}1}$; R380^{EBNA1} formed a salt bridge with D270$^{Imp_{\alpha}1}$ and hydrophobic/cation-π interactions with W231$^{Imp_{\alpha}1}$; R382^{EBNA1} was sandwiched between W184$^{Imp_{\alpha}1}$ and W142$^{Imp_{\alpha}1}$ and formed a hydrogen bond with Q181$^{Imp_{\alpha}1}$. These interactions were supplemented with hydrogen bonds between the main chain of EBNA1 and N235$^{Imp_{\alpha}1}$, N188$^{Imp_{\alpha}1}$, N146$^{Imp_{\alpha}1}$, W184$^{Imp_{\alpha}1}$ and W142$^{Imp_{\alpha}1}$.

3.2 Crystal structure of Impα1 bound to non-phosphorylated EBNA1 NLS peptide

As a control, we also determined the crystal structure of the NLS-binding ARM repeat domain of Impα1 bound to the non-phosphorylated NLS peptide of EBNA1 at 2.2 Å resolution (Table 1). The structure was refined to free and working *R*-factor values of 20.4% and 17.7%, respectively. As was the case in the co-crystal structure with the S385-phosphorylated NLS peptide, the non-phosphorylated NLS peptide bound to both minor and major NLS-binding sites of Impα1 (Fig. 2B). Residues 378-382 and 378-383 of the NLS peptide were identified unambiguously in the electron density map at the minor and major NLS-binding sites, respectively (Fig. 1C and 1D). The structures of S385-phosphorylated NLS peptide- and non-phosphorylated NLS peptide-Impα1 complexes superimposed very well with root mean square deviations of only 0.094 Å for all α carbon atoms of EBNA1 and Impα1. As shown in Fig. 2C and

2D, the two NLS peptides had essentially the same conformations when bound to Impα1. The only notable difference between the two peptides was that the electron density of residues 383-385 of non-phosphorylated NLS at the minor NLS-binding site was too weak to be modeled reliably (Fig. 1C), whereas these residues had well defined electron density in the case of S385-phosphorylated NLS (Fig. 1A). This indicates that phosphorylation of S385 can stabilize the conformation of these residues when bound to the minor NLS-binding site of Impα1.

3.3 Implications for the mechanism by which phosphorylation of EBNA1 NLS finely tunes the efficiency of nuclear import

Our structural data that non-phosphorylated EBNA1 NLS can bind to Impα1 provide a structural explanation for the observation that the non-phosphorylated NLS peptide can act as a functional signal to mediate nuclear import, albeit at a low efficiency [18]. Previous mutational analyses have shown that K379A and R380A substitutions greatly reduce nuclear import [18], and this is consistent with our structural data that these residues are involved in extensive interactions with Impα1 both at the major and minor NLS-binding sites.

An important implication from the co-crystal structures described above is that, although the phosphorylation of S385 of EBNA1 NLS is not required for the binding to Impα, it could strengthen the binding to Impα through electrostatic interaction at the minor NLS-binding site (but not at the major NLS-binding site) and thereby increase the efficiency of nuclear import. The phosphate group of $pS385^{EBNA1}$ did not form extensive hydrogen bonding network with Impα1 and instead, it formed only a long-range electrostatic interaction with $K392^{Imp_{\alpha}1}$ at the minor NLS-binding site. It therefore appears that this is not a high affinity phosphoserine binding, and

phosphorylation of $S385^{EBNA1}$ may make only a small contribution to the binding affinity to Impα, at least in the case of Impα1. In this context, an intriguing previous observation is that the binding affinity of Impα5 to the S385-phosphorylated EBNA1 NLS is significantly higher than that of Impα1 [18]. The residues of Impα1 that are involved in the recognition of the EBNA1 NLS are highly conserved among the Impα isoforms, and the only difference between Impα1 and Impα5 regarding the amino acid sequence in the EBNA1 NLS-binding sites is that K392 of Impα1 is arginine (R395) in Impα5. Generally, the guanidinium group of an arginine residue is well suited for interactions with a phosphate group by virtue of its planar structure and its ability to form multiple hydrogen bonds, and it has been reported that arginine can make substantially stronger salt bridges with phosphorylated amino acid side chains than lysine [40]. Therefore, the higher affinity of Impα5 to the S385-phosphorylated EBNA1 NLS could be due to the ability of R395 of Impα5 to provide a tight binding site for phosphoserine by making direct salt bridges with the phosphate group. However, this remains to be verified by structure determination of Impα5 bound to the S385-phosphorylated EBNA1 NLS.

To our knowledge, this study is the first to visualize the interaction between a nuclear transport receptor and a phosphorylated amino acid in a NLS by experimental structure determination. Interestingly, however, a previous molecular modeling and mutagenesis study suggested that R395 of Impα5 directly binds to phosphoserine in the bipartite NLS of human telomerase reverse transcriptase (hTERT) and thereby increases the efficiency of nuclear import of hTERT when the serine residue (S227) in the hTERT NLS is phosphorylated [41]. Thus, the interaction between the phosphorylated residue in a NLS and the basic residue (K392 of Impα1; R395 of Impα5) on ARM repeat 8 of Impα may be a general mechanism of up-regulation of nuclear import.

Conflicts of interest

The authors declare that they have no conflict of interest.

Acknowledgements

We thank the staff of Photon Factory for assistance during X-ray diffraction data collection.

References

[1] R.M. Longnecker, E. Kieff, J.I. Cohen, Epstein-Barr virus, in: D.M. Knipe, P.M. Howley (Eds.), Fields Virology, 6th ed., Lippincott-Williams and Wilkins, 2013, pp. 1898-1959.

[2] J.L. Yates, N. Warren, B. Sugden, Stable replication of plasmids derived from Epstein-Barr virus in various mammalian cells, Nature 313 (1985) 812-815.

[3] S. Lupton, A.J. Levine, Mapping genetic elements of Epstein-Barr virus that facilitate extrachromosomal persistence of Epstein-Barr virus-derived plasmids in human cells, Mol Cell Biol 5 (1985) 2533-2542.

[4] D. Reisman, J. Yates, B. Sugden, A putative origin of replication of plasmids derived from Epstein-Barr virus is composed of two cis-acting components, Mol Cell Biol 5 (1985) 1822-1832.

[5] D.R. Rawlins, G. Milman, S.D. Hayward, G.S. Hayward, Sequence-specific DNA binding of the Epstein-Barr virus nuclear antigen (EBNA-1) to clustered sites in the plasmid maintenance region, Cell 42 (1985) 859-868.

[6] D. Reisman, B. Sugden, trans activation of an Epstein-Barr viral transcriptional enhancer by the Epstein-Barr viral nuclear antigen 1, Mol Cell Biol 6 (1986) 3838-3846.

[7] T.A. Gahn, B. Sugden, An EBNA-1-dependent enhancer acts from a distance of 10 kilobase pairs to increase expression of the Epstein-Barr virus LMP gene, J Virol 69 (1995) 2633-2636.

[8] J.B. Wilson, J.L. Bell, A.J. Levine, Expression of Epstein-Barr virus nuclear antigen-1 induces B cell neoplasia in transgenic mice, EMBO J 15 (1996) 3117-3126.

[9] G. Kennedy, J. Komano, B. Sugden, Epstein-Barr virus provides a survival factor to Burkitt's lymphomas, Proc Natl Acad Sci U S A 100 (2003) 14269-14274.

[10] B. Gruhne, R. Sompallae, D. Marescotti, S.A. Kamranvar, S. Gastaldello, M.G. Masucci, The Epstein-Barr virus nuclear antigen-1 promotes genomic instability via induction of reactive oxygen species, Proc Natl Acad Sci U S A 106 (2009) 2313-2318.

[11] J.C. Hearing, A.J. Levine, The Epstein-Barr virus nuclear antigen (BamHI K antigen) is a single-stranded DNA binding phosphoprotein, Virology 145 (1985) 105-116.

[12] M. Polvino-Bodnar, J. Kiso, P.A. Schaffer, Mutational analysis of Epstein-Barr virus nuclear antigen 1 (EBNA 1), Nucleic Acids Res 16 (1988) 3415-3435.

[13] L. Petti, C. Sample, E. Kieff, Subnuclear localization and phosphorylation of Epstein-Barr virus latent infection nuclear proteins, Virology 176 (1990) 563-574.

[14] L. Frappier, M. O'Donnell, Overproduction, purification, and characterization of EBNA1, the origin binding protein of Epstein-Barr virus, J Biol Chem 266 (1991) 7819-7826.

[15] S.J. Duellman, K.L. Thompson, J.J. Coon, R.R. Burgess, Phosphorylation sites of Epstein-Barr virus EBNA1 regulate its function, J Gen Virol 90 (2009) 2251-2259.

[16] K. Shire, P. Kapoor, K. Jiang, M.N. Hing, N. Sivachandran, T. Nguyen, L. Frappier, Regulation of the EBNA1 Epstein-Barr virus protein by serine phosphorylation and arginine methylation, J Virol 80 (2006) 5261-5272.

[17] M.S. Kang, E.K. Lee, V. Soni, T.A. Lewis, A.N. Koehler, V. Srinivasan, E. Kieff, Roscovitine inhibits EBNA1 serine 393 phosphorylation, nuclear localization, transcription, and episome maintenance, J Virol 85 (2011) 2859-2868.

[18] R. Kitamura, T. Sekimoto, S. Ito, S. Harada, H. Yamagata, H. Masai, Y. Yoneda, K. Yanagi, Nuclear import of Epstein-Barr virus nuclear antigen 1 mediated by NPI-1 (Importin alpha5) is up- and down-regulated by phosphorylation of the nuclear localization signal for which Lys379 and Arg380 are essential, J Virol 80 (2006) 1979-1991.

[19] D. Gorlich, U. Kutay, Transport between the cell nucleus and the cytoplasm, Annu Rev Cell Dev Biol 15 (1999) 607-660.

[20] A. Kaffman, E.K. O'Shea, Regulation of nuclear localization: a key to a door, Annu Rev Cell Dev Biol 15 (1999) 291-339.

[21] J.D. Nardozzi, K. Lott, G. Cingolani, Phosphorylation meets nuclear import: a review, Cell Commun Signal 8 (2010) 32.

[22] M. Christie, C.W. Chang, G. Rona, K.M. Smith, A.G. Stewart, A.A. Takeda, M.R. Fontes, M. Stewart, B.G. Vertessy, J.K. Forwood, B. Kobe, Structural Biology

and Regulation of Protein Import into the Nucleus, J Mol Biol 428 (2016) 2060-2090.

[23] R.A. Pumroy, G. Cingolani, Diversification of importin-alpha isoforms in cellular trafficking and disease states, Biochem J 466 (2015) 13-28.

[24] Y. Miyamoto, K. Yamada, Y. Yoneda, Importin alpha: a key molecule in nuclear transport and non-transport functions, J Biochem 160 (2016) 69-75.

[25] R.F. Ambinder, M.A. Mullen, Y.N. Chang, G.S. Hayward, S.D. Hayward, Functional domains of Epstein-Barr virus nuclear antigen EBNA-1, J Virol 65 (1991) 1466-1478.

[26] N. Fischer, E. Kremmer, G. Lautscham, N. Mueller-Lantzsch, F.A. Grasser, Epstein-Barr virus nuclear antigen 1 forms a complex with the nuclear transporter karyopherin alpha2, J Biol Chem 272 (1997) 3999-4005.

[27] A.L. Kim, M. Maher, J.B. Hayman, J. Ozer, D. Zerby, J.L. Yates, P.M. Lieberman, An imperfect correlation between DNA replication activity of Epstein-Barr virus nuclear antigen 1 (EBNA1) and binding to the nuclear import receptor, Rch1/importin alpha, Virology 239 (1997) 340-351.

[28] S. Ito, M. Ikeda, N. Kato, A. Matsumoto, Y. Ishikawa, S. Kumakubo, K. Yanagi, Epstein-barr virus nuclear antigen-1 binds to nuclear transporter karyopherin alpha1/NPI-1 in addition to karyopherin alpha2/Rch1, Virology 266 (2000) 110-119.

[29] J. Nardozzi, N. Wenta, N. Yasuhara, U. Vinkemeier, G. Cingolani, Molecular basis for the recognition of phosphorylated STAT1 by importin alpha5, J Mol Biol 402 (2010) 83-100.

[30] M.R. Fontes, T. Teh, B. Kobe, Structural basis of recognition of monopartite and bipartite nuclear localization sequences by mammalian importin-alpha, J Mol Biol 297 (2000) 1183-1194.

[31] M.D. Winn, C.C. Ballard, K.D. Cowtan, E.J. Dodson, P. Emsley, P.R. Evans, R.M. Keegan, E.B. Krissinel, A.G. Leslie, A. McCoy, S.J. McNicholas, G.N. Murshudov, N.S. Pannu, E.A. Potterton, H.R. Powell, R.J. Read, A. Vagin, K.S. Wilson, Overview of the CCP4 suite and current developments, Acta Crystallogr D Biol Crystallogr 67 (2011) 235-242.

[32] A. Vagin, A. Teplyakov, Molecular replacement with MOLREP, Acta Crystallogr D Biol Crystallogr 66 (2010) 22-25.

[33] M. Marfori, T.G. Lonhienne, J.K. Forwood, B. Kobe, Structural basis of high-affinity nuclear localization signal interactions with importin-alpha, Traffic 13 (2012) 532-548.

[34] P. Emsley, K. Cowtan, Coot: model-building tools for molecular graphics, Acta Crystallogr D Biol Crystallogr 60 (2004) 2126-2132.

[35] G.N. Murshudov, P. Skubak, A.A. Lebedev, N.S. Pannu, R.A. Steiner, R.A. Nicholls, M.D. Winn, F. Long, A.A. Vagin, REFMAC5 for the refinement of macromolecular crystal structures, Acta Crystallogr D Biol Crystallogr 67 (2011) 355-367.

[36] P.D. Adams, P.V. Afonine, G. Bunkoczi, V.B. Chen, I.W. Davis, N. Echols, J.J. Headd, L.W. Hung, G.J. Kapral, R.W. Grosse-Kunstleve, A.J. McCoy, N.W. Moriarty, R. Oeffner, R.J. Read, D.C. Richardson, J.S. Richardson, T.C. Terwilliger, P.H. Zwart, PHENIX: a comprehensive Python-based system for macromolecular structure solution, Acta Crystallogr D Biol Crystallogr 66 (2010) 213-221.

[37] V.B. Chen, W.B. Arendall, 3rd, J.J. Headd, D.A. Keedy, R.M. Immormino, G.J. Kapral, L.W. Murray, J.S. Richardson, D.C. Richardson, MolProbity: all-atom structure validation for macromolecular crystallography, Acta Crystallogr D Biol Crystallogr 66 (2010) 12-21.

[38] S. McNicholas, E. Potterton, K.S. Wilson, M.E. Noble, Presenting your structures: the CCP4mg molecular-graphics software, Acta Crystallogr D Biol Crystallogr 67 (2011) 386-394.

[39] W.L. DeLano, The PyMOL Molecular Graphics System, 2002. http://www.pymol.org.

[40] D.J. Mandell, I. Chorny, E.S. Groban, S.E. Wong, E. Levine, C.S. Rapp, M.P. Jacobson, Strengths of hydrogen bonds involving phosphorylated amino acid side chains, J Am Chem Soc 129 (2007) 820-827.

[41] S.A. Jeong, K. Kim, J.H. Lee, J.S. Cha, P. Khadka, H.S. Cho, I.K. Chung, Akt-mediated phosphorylation increases the binding affinity of hTERT for importin alpha to promote nuclear translocation, J Cell Sci 128 (2015) 2287-2301.

Figure legends

Fig. 1. The electron density map of (A, B) S385-phosphorylated and (C, D) non-phosphorylated EBNA1 NLS peptides bound to Impα1. The $2F_O–F_C$ electron density maps (contoured at 1σ) covering the NLS peptides at (A, C) the minor NLS-binding site and (B, D) the major NLS-binding site are shown in blue mesh with the refined models of the EBNA1 NLS peptides.

Fig. 2. Structures of Impα1 bound to the EBNA1 NLS peptides. (A) Overall structure of ΔIBB Impα1 (ribbon representation) bound to S385-phosphorylated EBNA1 NLS peptide (stick representation) (PDB code, 5WUM). (B) Overall structure of ΔIBB Impα1 (ribbon representation) bound to non-phosphorylated EBNA1 NLS peptide (stick representation) (PDB code, 5WUN). (C, D) Overlay of the S385-phosphorylated (stick representation with yellow carbons) and non-phosphorylated (stick representation with pink carbons) NLS peptides bound to Impα1 at (C) the minor NLS-binding site and (D) the major NLS-binding site.

Fig. 3. Recognition of the S385-phosphorylated EBNA1 NLS by Impα1. (A, B) Close-up views of the interactions between Impα1 (ribbon representation in light gray) and the S385-phosphorylated EBNA1 NLS peptide (stick representation with light blue carbons) at (A) the minor NLS-binding site and (B) the major NLS-binding site. (C) Molecular surface of Impα1 at the minor NLS-binding site colored by electrostatic potential (blue, positive; red, negative; white, neutral). (D) Schematic illustration of the interactions between Impα1 and the S385-phosphorylated EBNA1 NLS at the minor NLS-binding site. Dashed lines represent hydrogen bonds or salt bridges or long-range electrostatic interactions.

Table 1. Crystallographic statistics.

Crystal	ΔIBB Impα1 bound to S385-phosphorylated NLS of EBNA1	ΔIBB Impα1 bound to non-phosphorylated NLS of EBNA1
Data collection		
Space group	$P2_12_12_1$	$P2_12_12_1$
Unit cell dimensions		
a, *b*, *c* (Å)	77.91, 90.30, 99.63	78.51, 90.18, 98.89
α, *β*, *γ* (degree)	90, 90, 90	90, 90, 90
Wavelength (Å)	0.98	0.98
X-ray source	Photon Factory BL-17A	Photon Factory BL-17A
Resolution range (Å)[a]	41.97-2.00 (2.05-2.00)	28.80-2.20 (2.27-2.20)
No. of measured reflections[a]	288684 (16841)	218370 (16032)
No. of unique reflections[a]	48181 (3485)	36317 (3083)
Completeness (%)[a]	99.9 (99.3)	99.9 (97.3)
R_{merge} (%)[a]	5.9 (86.3)	8.7 (99.0)
Mean $I/\sigma(I)$[a]	19.0 (1.8)	14.1 (1.8)
Mean *I* half-set correlation CC(1/2)[a]	0.999 (0.653)	0.998 (0.599)
Multiplicity[a]	6.0 (4.8)	6.0 (5.2)
Refinement		
Resolution range (Å)[a]	41.97-2.00 (2.04-2.00)	28.80-2.20 (2.26-2.20)
R_{work} (%)[a]	18.6 (28.2)	17.7 (27.6)
R_{free} (%)[a]	21.2 (33.0)	20.4 (31.6)
No. of atoms		
Protein	3363	3340
Water	258	174
No. of amino acids	440	437
Mean *B* factor (Å^2)		
ΔIBB Impα1	42.6	48.2
EBNA1 NLS (major site)	50.4	57.4
EBNA1 NLS (minor site)	63.5	61.9
Water	48.5	50.1
RMSD from ideality		
Bond lengths (Å)	0.004	0.004
Bond angles (degree)	0.630	0.683
Protein geometry[b]		
Rotamer outliers (%)	0	0
Ramachandran favored (%)	99.1	98.4
Ramachandran outliers (%)	0	0
Cβ deviations > 0.25 Å (%)	0	0
MolProbity score (percentile)	1.28 (99)	1.15 (100)
PDB code	5WUM	5WUN

[a] Values in parentheses are for the highest-resolution shell.

[b] MolProbity [37] was used to analyze the structures.

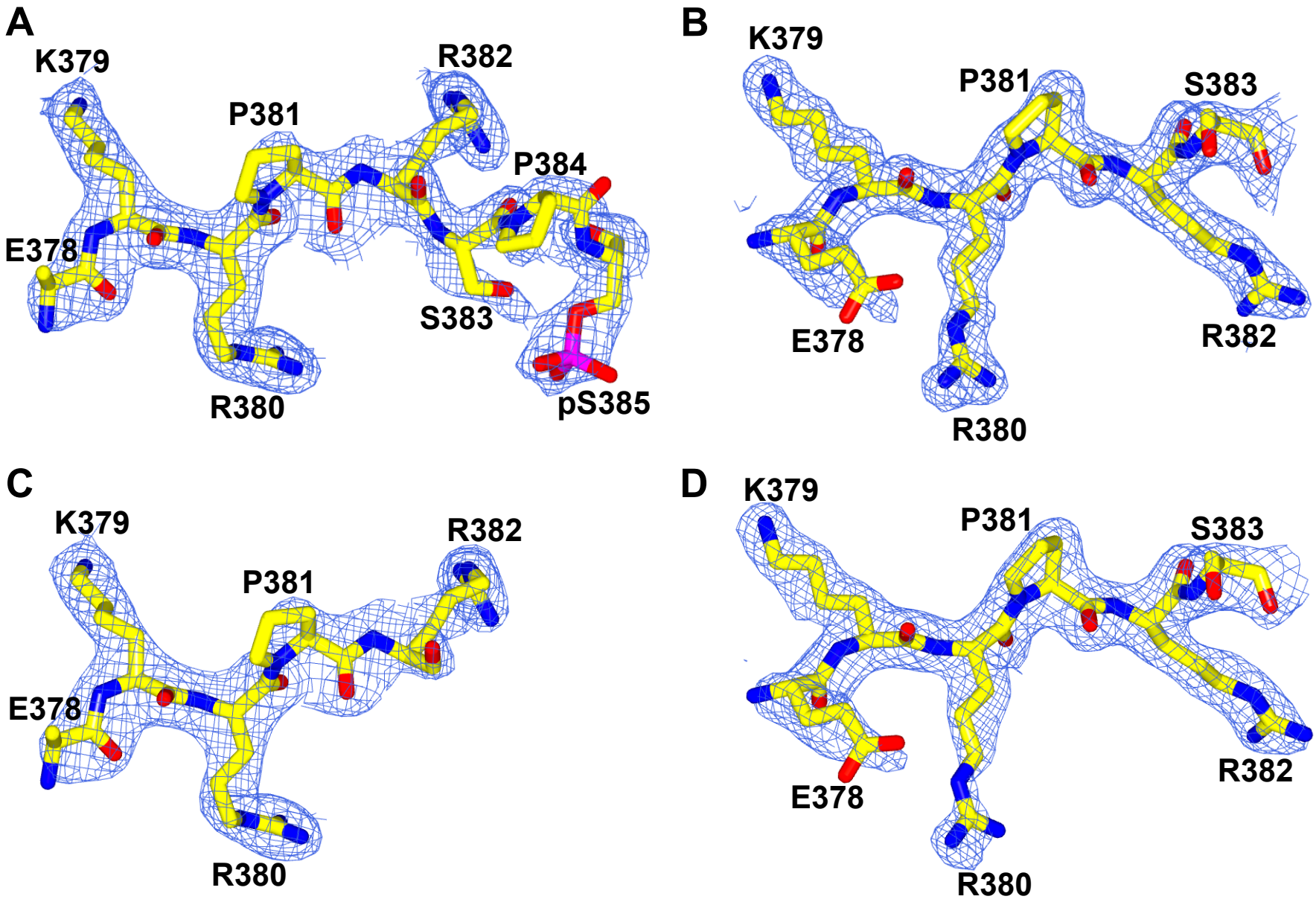
A
K379
R382
P381
P384
E378
S383
R380
pS385
B
K379
P381
S383
E378
R382
R380
C
K379
R382
P381
E378
R380
D
K379
P381
S383
R382
E378
R380

Fig. 1

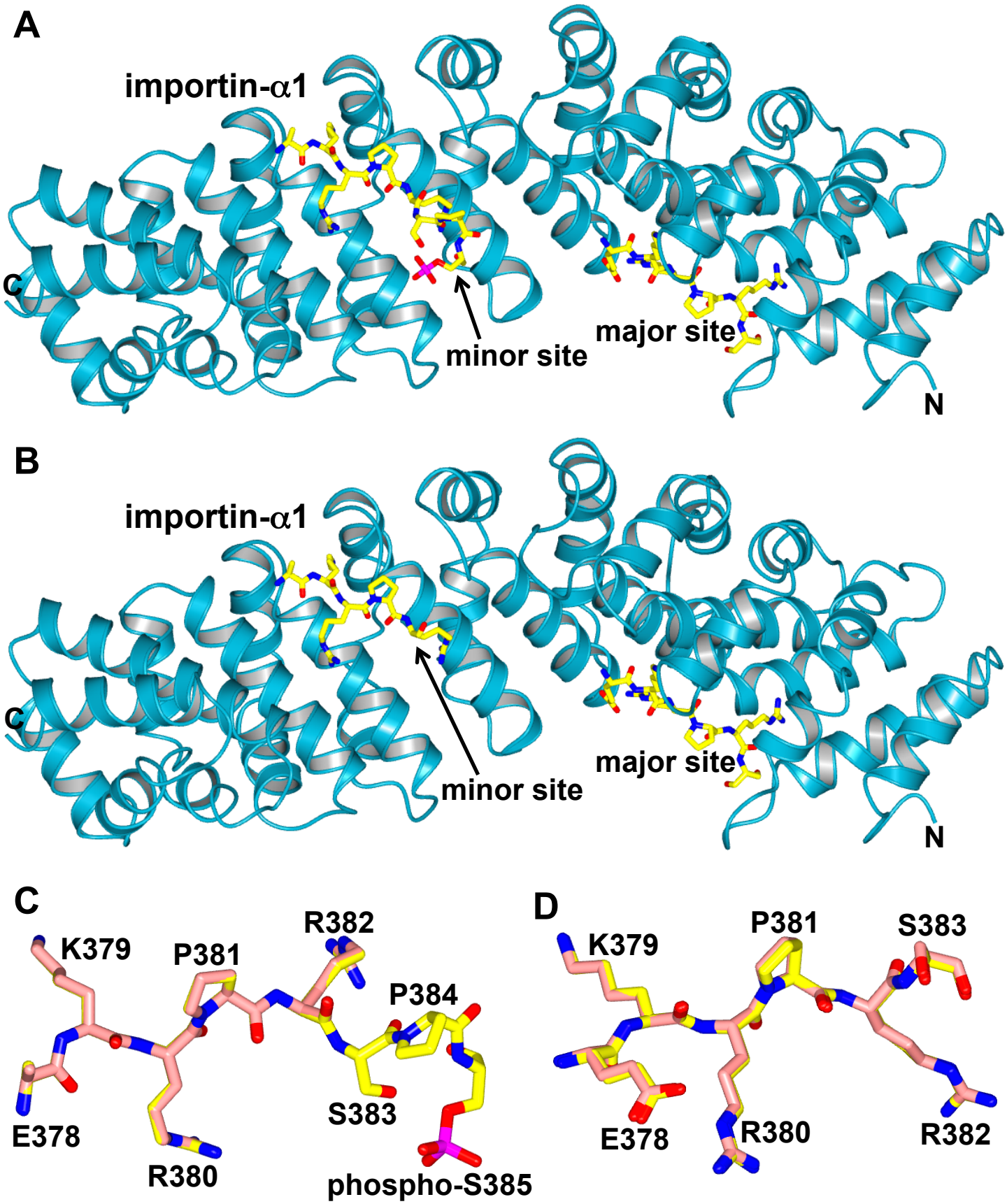
A
importin-α1
C
minor site
major site
N
B
importin-α1
C
minor site
major site
N
C
K379
P381
R382
P384
S383
E378
R380
phospho-S385
D
K379
P381
S383
E378
R380
R382

Fig. 2

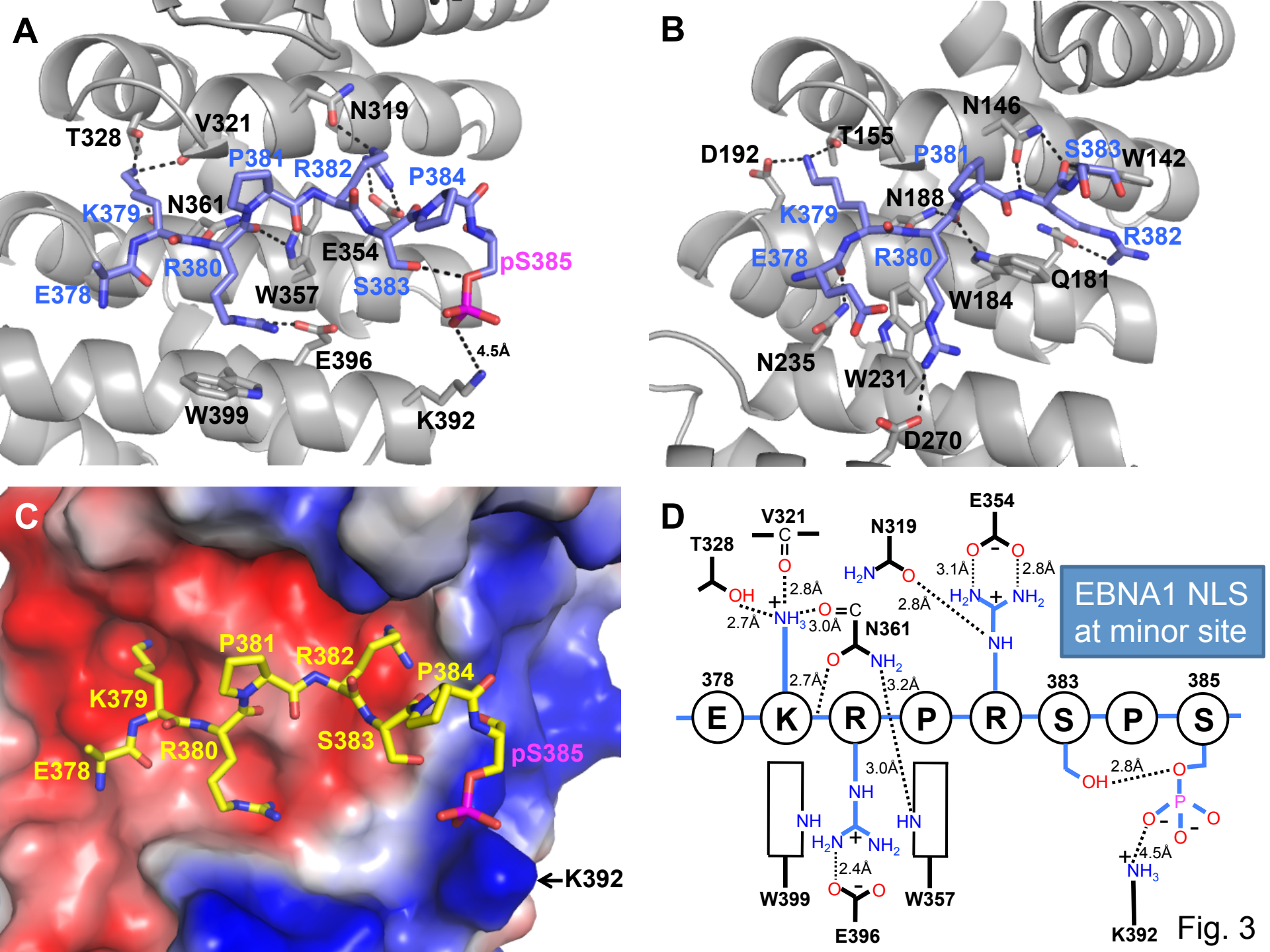
A
T328
V321
N319
P381
R382
P384
K379
N361
E354
R380
pS385
E378
W357
S383
E396
4.5Å
W399
K392
B
N146
T155
D192
P381
S383
W142
N188
K379
R382
E378
R380
Q181
W184
N235
W231
D270
C
P381
R382
P384
K379
S383
E378
R380
pS385
K392
D
V321
T328
N319
E354
2.8Å
3.1Å
2.8Å
2.7Å
3.0Å
N361
2.8Å
2.7Å
3.2Å
3.0Å
2.8Å
2.4Å
4.5Å
378
383
385
E
K
R
P
R
S
P
S
W399
W357
E396
K392
EBNA1 NLS
at minor site
Fig. 3